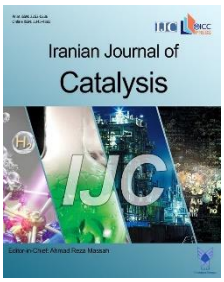

Volume 15, Issue 4, (2025) Article (1-13)

Iranian Journal of Catalysis (IJC)

https://doi.org/10.57647/j.ijc.2025.1504.40

Greener Synthesis of MNPs Using *Achyranthesaspera Leaf* Extract: Compared Photocatalytic Activity, Reduction, and Adsorption Investigations for the Environmental Remediation

Raju Shekhanavar, Kantharaju Kamanna *

Department of chemistry, Rani channamma University, Belagavi, Karnataka, 591156, India

***Corresponding author:** kk@rcub.ac.in

Original Research

Received:
30 April 2025

Revised:
17 June 2025

Accepted:
10 July 2025

Published online:
5 November 2025

Published in issue:
31 December 2025

Abstract

A greener method described using water extract leaves of *Achyranthesaspera* plant (Uttarani plant) employed for iron oxide nanoparticles (MNPs) preparation, and demonstrated application of the prepared NPs for dye removal from the contaminated water by photo chemically. The *Achyranthes aspera* leaves were used for the first time for the iron oxide NPs preparation as a biogenic method. The phytochemical present in the extracted solution served as a reducing agent, facilitating NPs formation. The prepared MNPs homogeneity was examined by FT-IR, UV-Vis, XRD, HR-SEM, and VSM analyses. Further, these MNPs were utilized for the decolourization of the industrial effluent (IE) and methylene blue (MB), and the catalytic reduction properties of 4-NA to 4-AA were evaluated. The decolourization of the MB and IE was monitored by UV-Vis, and followed by kinetic comparisons and HR-MS analysis, which revealed that adsorption takes place on the surface.

Keywords: Iron oxide; Magnetic nanoparticles; Achyranthesaspera; Leaf extract; Industrial effluent; Methylene blue

1. Introduction

Development of a special category of nanomaterial called magnetic nanoparticles (abbreviated MNPs, Fe_3O_4) has attracted much more attention due to their unique applications in the area of material science, biomedical (MRI), environmental remediation, and so forth [1]. The MNPs were found to be excellent photocatalysts and adsorbents, which had been reported by the researchers [2] because of their exceptional magnetic properties and a second-best part, simple to isolate in a photocatalysis response open at the highest point of responsiveness utilizing an external magnet [3]. As a result, it generates lower secondary waste and can also be considered for the next generation of photocatalysis [4]. Among all photocatalysis, the removal of dye-contaminated water has intrigued significant interest because it is the most effective technique and well-guaranteed for environmental protection [5-10]. While several industrial effluents that contain dye are often toxic & carcinogenic and cause serious problems due to environmental pollution, along with being harmful to human beings [11]. The leather, textile, paper, food colouring, and cosmetic industries are major contributors to water pollution via effluents in the water stream rich in organic dyes and pigments [12]. This mainly creates water in a highly polluted form, as even a low concentration of dye can create an excessive amount of pollution of water, and consumption of such dyed water leads to intolerable levels of pollution to human health, as well as to aquatic studies [13-16]. Furthermore, the water pollution itself is causing a slow and steady decrease in clean and potable impersonal or public drinking water [17]. Therefore, nowadays, wastewater management is becoming one of the challenging research areas among top priorities [18]. Hence, waste water containing organic dye removal is necessary for the betterment of the aquatic system [19].

Waste water containing dye is of a resistant, harsh condition and biodegradation, making this property hard to disintegrate from water [20]. Various waste water treatment techniques that have evolved are adsorption, coagulation/sedimentation [21], filtration [22-25], chemical oxidation [26], and photocatalysis [27]. Photocatalysis is a green chemistry process that makes use of solar energy for catalytic reactions [28]. Therefore, the use of photocatalysts was widely studied in semiconductor or light-absorbing materials that can induce dye degradation or adsorption from the wastewater [29].

There is still greater potential for the development of sustainable, cost-effective photocatalysts for dye degradation and MNPs synthesis [30]. Different MNPs nanoparticles in size and distribution, other than application of photocatalysis, adsorbent, and biological, were reported using plant extract solution-based preparation in the literature (Table 1). *Achyranthesaspera* common name prickly chaff flower, chaff-flower and devils horsewhip family of *Amarantaceae*. This plant is endemic worldwide [39]. They can be found growing in a lot of places, and they are endemic to some sites (Figure S1). The bark is also utilised in the folk medicine of countries as distant as Australia, India, and Kenya. The juice of this plant is used as a potent ingredient for the mixture of wall plaster [40]. The leaf extract was also explored for silver, copper, and gold NPs synthesis [41-45]. Textile industries playing major consumers of dyestuff globally made, and one lakh tons more than of unbound dye discharged into the environment. Dye is a colour substrate that chemically binds to the substrate, on which it is applied [46]. Dye, unlike organic compounds which are able to absorb light in the visible spectrum owing to at least one chromosphere with a conjugated system [47].

Various photocatalysts have been discovered and reported for methylene blue degradation and industrial effluent treatments [48-50]. Further in this work described greener process Fe_3O_4 synthesis using *Achyranthes aspera* leaf extract contains phytochemical responsible for stabilizing and reduction processes of MNPs. The obtained Fe_3O_4 NPs were characterized completely and exhibited photocatalytic abilities for the decolourization of the MB dye and industrial effluent.

2. Experimental

2.1. General

Materials: The required chemicals to carry out this work were procured from Avra and SD-Fine Chemicals and used as received. FT-IR spectra collected in a BRUKER ALPHA II spectrometer (Eco-ATR-FT-IR). XRD data collected in a PANalytical X-pert PRO.

TESCAN/Bruker for surface morphology and elemental mapping (SEM/FESEM, EDS)-MIRA-3 (FESEM), and Quantax-200. Magnetic measurements were acquired using a VSM (Vibrating Sample Magnetometer). Waters (SynaptG2) for HR-MS measurement was used.

2.2. Water extract of *Achyranthesaspera* preparation

Fresh leaves clipped from the university garden were washed properly with water and soaked for 30 minutes in distilled water to eliminate debris and soil. The aqueous extract was prepared at 45 °C by chopping 25 g of young leaves into small pieces and transferring them to a conical flask (250 mL), then adding distilled water (100 mL), boiling the mixture (leaf &water) for about 30 minutes. The obtained solution was filtered (Whatmann No.1) after cooling and used as such for the preparation of iron oxide NPs.

Table 1. Comparison of green method-derived Iron oxide NPs for dye degradation.

Plant source	Shape	Size (nm)	Dye	Reference
Platanus orientalis	Spherical	38	MR	[31]
Zanthoxylum armatum	Spherical	17	MO	[32]
Kappaphycus alvarezi	Irregular	14.7	MY	[33]
Ruellia tuberosa	Cubic	52.8	MO	[34]
Artemisia vulgaris leaf	Spherical	30	ET	[35]
Banana peel	Needles	60	RB	[36]
Fenugreek Seed	Spherical	100	CR	[37]
Kappaphycus alvarezii	Spherical	21.8	MO	[38]
Achyranthesaspera	ovate	30	MB & IE	(Present work)

2.3. Preparation of Fe_3O_4 NPs

Weighed 3 g of each $FeSO_4.7H_2O$ and $FeCl_3.6H_2O$ in a 250 mL beaker, and added 50mL of the above leave extract, warmed in a water bath for 45 min at 80-85°C, then cooled to room temperature, and an excess of 2% NaOH solution was added dropwise till the black precipitate ceased. The mixture was left to cool to rt, and a black solid was collected after several washes with water and alcohol using external magnetic separation.

Afterwards, the resulting product was dried and calcinated in the muffle furnace.

2.4. Photocatalysts test

In separate beakers, 0.01 g of Fe_3O_4 was added to 100 mL of a 20 mg/L MB dye solution. The mixture was stirred in the dark for 30 min; this step allowed for adsorption equilibrium to be reached. Once this period was over, they were exposed to sunlight for over 2 hrs at 30, 60, 90, and 120-minute intervals. Withdrawn each time 5 mL aliquots from the reaction beaker and centrifuged. The supernatant containing MB dye was analysed using UV-Vis at 534 nm to determine dye concentration.

2.5. Catalytic test

To study the catalytic properties of the prepared Fe_3O_4, we use it in the reduction of 4-nitroaniline (4-NA) to 4-phenylenediamine (4-AA). In a typical reaction, 400 µl of 1mM 4-NA aqueous solution, 400 µl of 10 mM NaBH4 aqueous solution, and 200 µl of Fe_3O_4 aqueous suspension were dispersed in 2 mL of water. The reduction reaction was monitored through a UV-Vis in a quartz cuvette with 10 mm path length and with freshly made solutions. The nanoparticles were separated from the solution by simply applying an external magnetic field and washed twice with 2 times distilled water.

3. Results and Discussion

3.1. Spectral analysis of Fe_3O_4 NPs

The present work describes Fe_3O_4 NPs synthesis using a biogenic method with the leaf extract of Achyranthes aspera, shown in Figure S2.

3.1.1. *FT-IR of Fe_3O_4*

A strong peak at 599 cm^{-1} is attributed to Fe-O tetrahedral in the spinel structure, as it has strong absorption by iron oxide. The significant absorption band occurring around 1633 cm^{-1} turns out to be ascribed to the OH bending of (H_2O) physically adsorbed. A strong peak at 3333cm^{-1} for O-H stretching water present on the surface of the Fe_3O_4, a weak band has been observed at 1097 cm^{-1}, which arises from C-O stretching of the surface carbon layer (Figure 1).

In Figure 2a, UV-Vis showed at 320 nm, which confirmed the formation of Fe_3O_4, as this was a characteristic feature of the iron oxide NPs formation. Also, other researchers reported that Fe_3O_4 peaks are normally found between 300 and 350nm. This also depends on the phytochemicals present in the biogenic extract, which are reducing agents.It is known that iron oxide NPs generally absorb a certain amount of UV radiation, which is caused by the movement of electrons from the valence band to the conduction band. The band gap was also measured through the Tauc plot, where it was found to be 3.75 eV (Figure 2b). The morphological analysis of this material through SEM/EDS for the plant-derived Fe_3O_4 was conducted to obtain more information.

3.1.2. *XRD of Fe_3O_4*

This X-ray diffraction technique is an analytical tool that provides the crystallinity nature of the materials or composition of the materials along with functional group information [51]. It is a standout amongst most useful characterization techniques in the materials and solid-state science [52].

XRD data obtained for Fe_3O_4 prepared showed at 31.4, 36.7, 44.3, 52.5, 58.6 and 63.8° 2Θ are indexed to (111), (202), (311), (222), (404) and (602) planes of Fe_3O_4, respectively with JCPDS No [39-1346] [53] (Figure 3).

3.1.3. *HR-SEM of Fe_3O_4*

The topography of the prepared Fe_3O_4 surface is shown in Figures 4a ,b. The SEM image clearly shows that the product comprises spheres having uniform flower-like architecture, and the sphere surface distinctly displays a designed flower-like structure, which is formed by a large number of nano sheets [54]. Also investigated was the surface morphology and elemental mapping of prepared Fe_3O_4 (Figure 4c).The above image clearly shows the fine particle size distribution of Fe_3O_4 ranging from 30-70 nm (calculated by Scherrer equation), and the major presence of Fe as an elemental constituent. The elemental mapping also indicates the good dispersion of the Fe_3O_4, Fe, and oxygen elements were further identified from EDS (Figure 5). The Au peak in the EDS spectrum was present for all samples, as they were all sputtered with gold, and the Fe peak was visible everywhere due to the background.

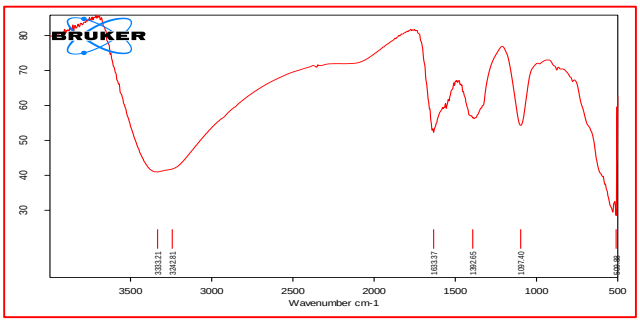

Figure 1. FT-IR of Fe_3O_4

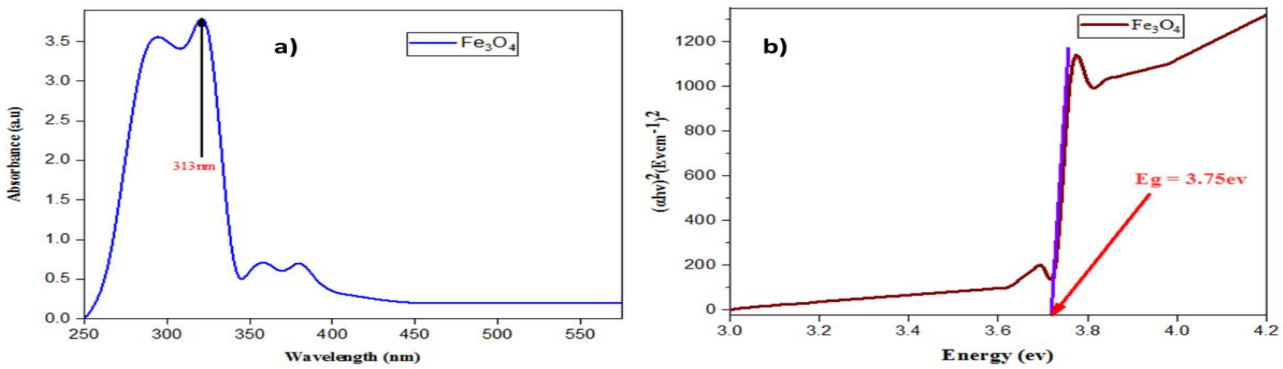

Figure 2. a)UV-visible plots of Fe_3O_4, b) Taucs plots of Fe_3O_4

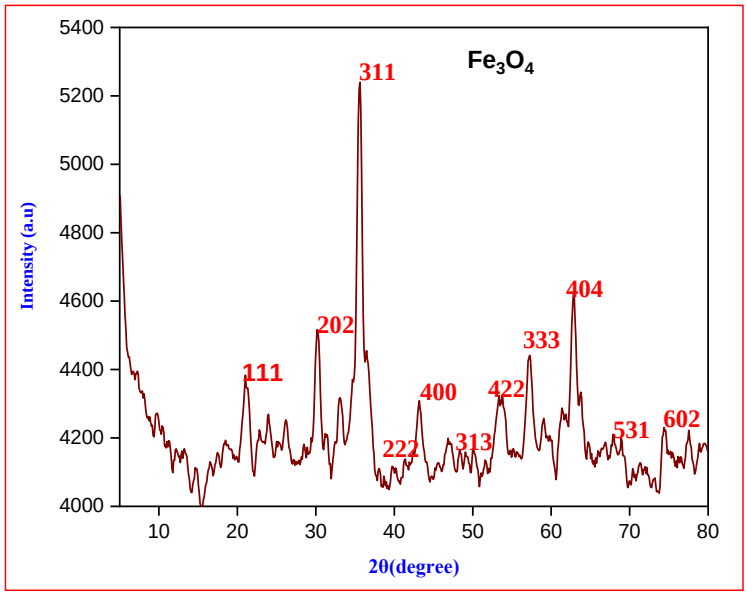

Figure 3. XRD of Fe_3O_4

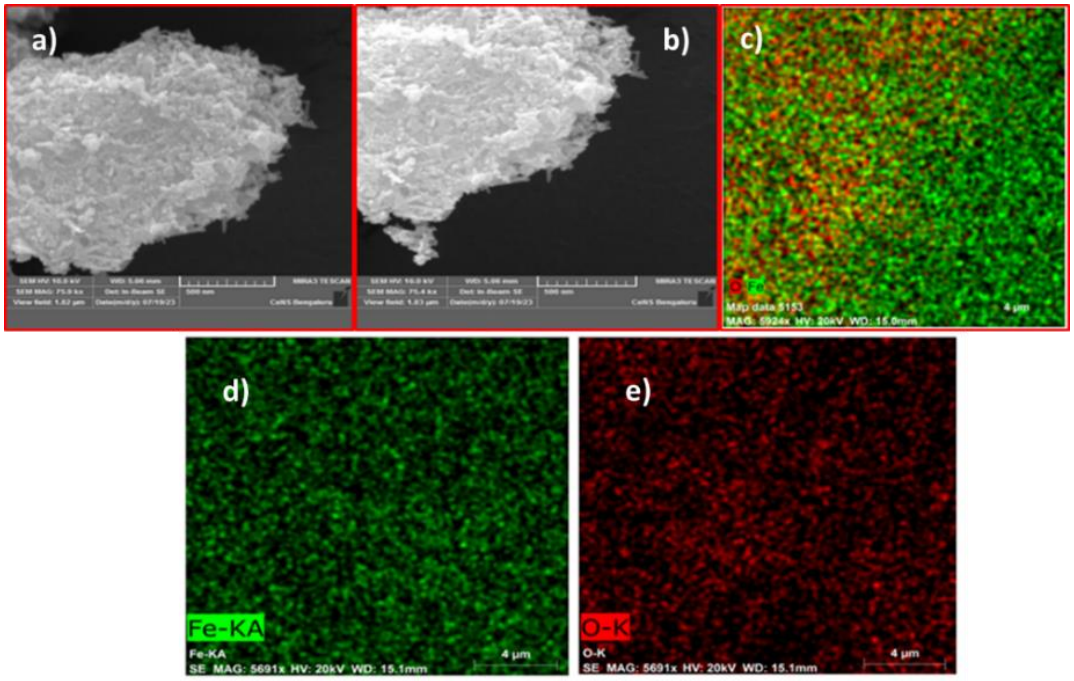

Figure 4. a-e. SEM of Fe_3O_4 NPs (5a & b); 5c, d, e. MNPs elemental mapping

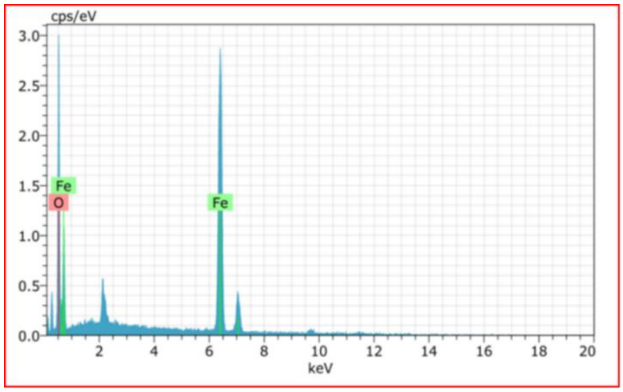

Element	Series	unn. C [wt.%]	norm. C [wt.%]	Atom. C [at.%]	Error (3 Sigma) [wt.%]
Oxygen	K-series	24.17	28.36	58.02	11.06
Iron	K-series	61.05	71.64	41.98	5.17
	Total:	85.22	100.00	100.00	

Figure 5. MNPs EDX profile

3.1.4. *HR-TEM-SAED analysis*

The TEM-SAED analysis was used to study the morphological characteristics and microstructural features of the synthesized Fe_3O_4 MNPs. The images showed an echinus-like morphology with an average particle size of around 35 nm, which agrees with XRD data associated with a relatively uniform particle size distribution. It was observed that lattice planes (inter planar spacing of 224 pm) correspond to the Fe_3O_4 planes (110). The SAED pattern is a series of diffraction rings indicating the polycrystalline nature. These diffraction rings can also be the plane of Fe_3O_4 crystallography, further supporting the phase purity associated with the nanoscale structures obtained (Figure 6).

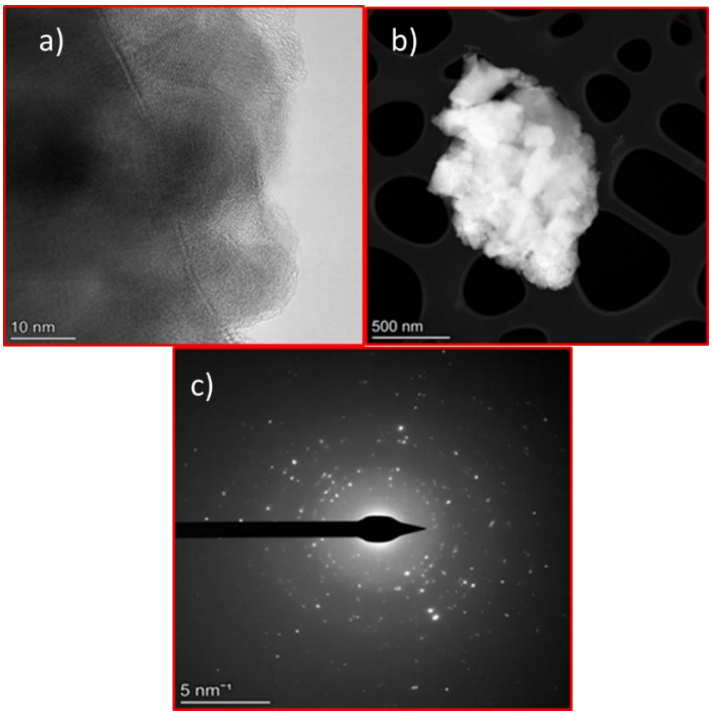

Figure 6. HR-TEM image of a) 10 nm & b) 500 nm, and c) SAED image of Fe_3O_4 MNPs

3.1.5. *VSM of Fe_3O_4*

A series of magnetic measurements were carried out for the prepared MNPs at rt (room temperature) using a VSM magnetic field external value from -1T to +1T (Figure 7).

To probe the corresponding properties of the resultant powder, including saturation magnetization. (Ms (emu/g), 36.11), residual magnetism [Mr(emu/g), 0.23], coercivity [Hc(Oe), 347.03] and magnetic susceptibility [X(emu /g.Oe), 0.00415]. It is quite be seen, where the value of Ms changed from 36.11 to be 0.00415 emu/g, this resembles magnetic behavior due to iron oxide, however on other edge it gives rise for certain saturation magnetism because of Fe^{3+} ions replaced with free Fe^{2+} ions.

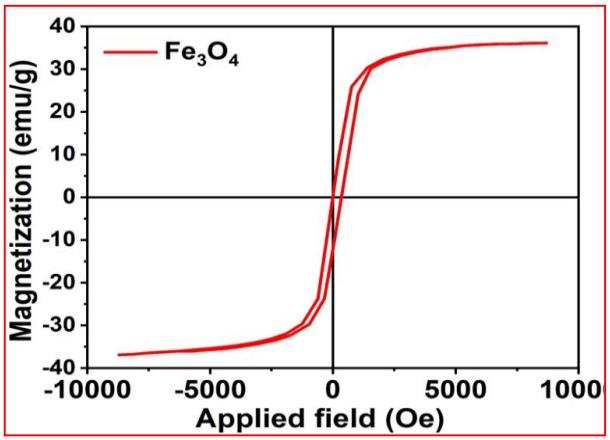

Figure 7. Magnetization curves of the Fe_3O_4

3.1.6. *Removal of MB dye monitored by UV-Vis*

MB dye was prepared in the lab, and 20 ppm was used for all experiments. The decolorization of the MB dye was spectrophotometrically monitored at λ_{max}= 664 nm using 1mL of test solution (Figure S3). Experimental set-up taken five beakers of the same volume containing 100 mL and each one with 10 mL of 20 ppm prepared MB solution, and (10 mg) Fe_3O_4 placed for required time interval of 30 min under sunlight (Figure 8), before catalysts adding to MB, and after catalyst adding UV-Vis spectra appended in Figure S4.

3.1.7. *Industrial effluent sample treatment*

It was monitored by the λ_{max} by UV-Vis absorption at 676 nm using IE samples before catalysts, and tested photodegradation of IE collected from the nearest textile industry under the above reaction conditions (Figures S5 & S6) in 30 min intervals, after the catalyst was added (Figure 9).

3.1.8. *Reduction of 4-nitroaniline*

The synthesized Fe_3O_4 catalytic properties were tested for 4-nitroaniline (4-NA) reduction with $NaBH_4$ at rt, and reaction was monitored by UV-Vis (Scheme 1). The reduction of 4-nitroaniline to 4-phenylenediamine achieved using MNPs as catalysis showed in Scheme 2. In Figure 10a presented UV-Vis absorption spectrum of 4-NA alone. The n → π* and π → π* type of transitions observed at the absorption peaks of 317 nm and 400 nm for an aqueous solution of 4-NA. The 4-NA solution is light yellow and changes to dark brown with NaBH4. The change in colour is associated with modulation of the highest absorption peak from 317 nm to 400 nm as a result of the nitro group reduction (Figure 10b). No reduction observed without the catalysts, in the presence of $NaBH_4$. Contrary, increment of Fe_3O_4 NPs added reduces the intensity λ_{max} ~400 nm, which corresponded to the formation of 4-AA.

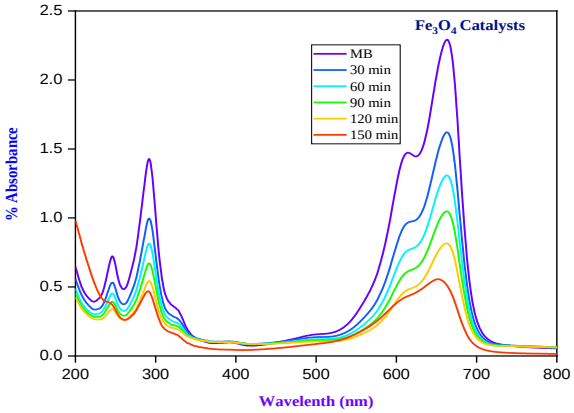

Figure 8. UV-Vis spectra of MB with Fe_3O_4

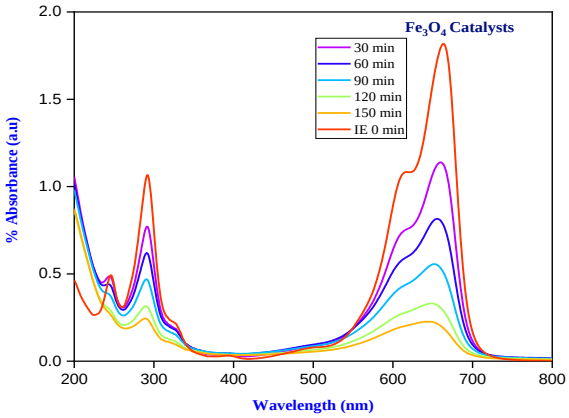

Figure 9. UV-Vis of IE with Fe_3O_4

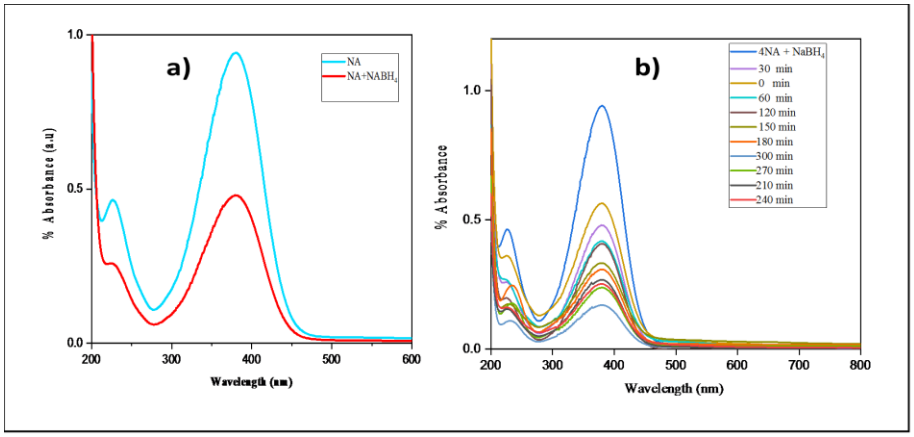

Figure 10. UV-Vis of: a) 4-NA alone & with NaBH4 without catalysts (reaction condition: 4-NA= 2mL (0.20 mM), NaBH4=100 µL (75 mM); b) Time-dependent 4-NA in NaBH4 with catalyst (reaction condition: 4-NA=2 mL (0.20 mM), NaBH4=100 µL (75 mM), catalyst=10 mg

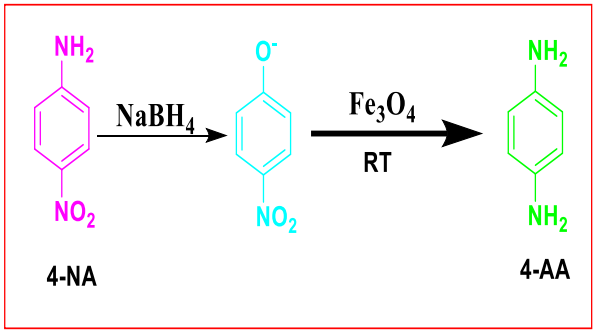

Scheme 1. Catalytic reduction of 4-NA to 4-AA

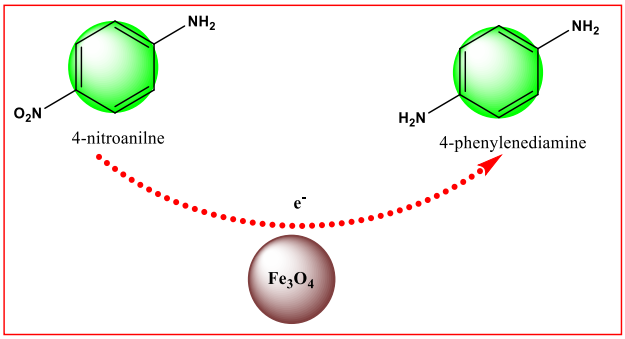

Scheme 2. Reaction of 4-NA to 4-AA reduction

3.1.9. *Reduction of MB and IE*

Further studied MB and IE reduction using $NaBH_4$ at rt employing iron oxide prepared, and reaction was monitored by UV-Vis spectra for MB and IE reduction in the presence of Fe_3O_4 and $NaBH_4$ or without MNPs (Figures S7 & S8). In this study, absorption of MB appeared at 664 nm and 280 nm (conjugated $\pi \rightarrow \pi^*$ transition), IE attained at 676 nm and 285 nm by comparing it with the reference compound to identify $n \rightarrow \pi^*$, and $\pi \rightarrow \pi^*$ transition, respectively [54]. There is no change in the absorption peak at 664 and 676 nm with the increased concentration of $NaBH_4$ added into the MB and IE dye. These observations confirmed that MB and IE cannot be reduced by $NaBH_4$ alone because of the very large potential difference in reduction potentials between MB, IE, and $NaBH_4$ [55]. Nevertheless, as the catalyst was dropped into the solution of MB, IE, and $NaBH_4$, the progressive decrease in the intensity at 664 nm and 676 nm was observed (Scheme 3).

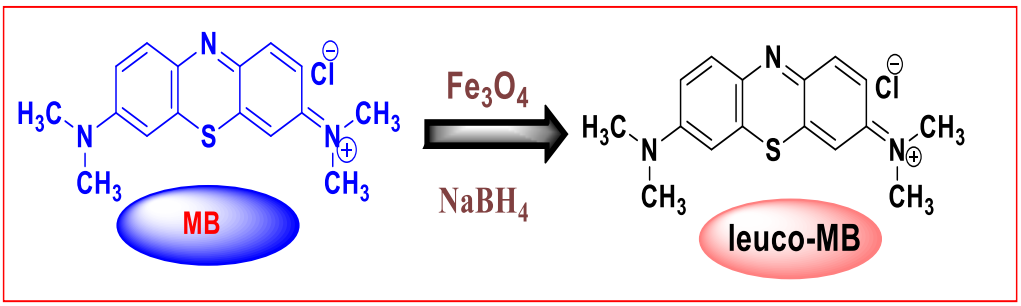

Scheme 3. Catalytic reduction of MB to LMB

The same peak in diffused reflectance spectrum is noted at 600 to 610 nm, corresponding directly to the reduction of MB and IE dye, with complete reduction taking place from colorimetric studies in 6-8 min [55]. Due to the decrease of absorbance at 660 nm for MB, a new peak appears at 350 nm, and its intensity increases with time due to leuco-MB generation. Disadvantageously, the remaining $NaBH_4$ concentration is higher than 0.025 M, and especially when the 2 mL MB (10 ppm) solution is used in catalyst studies, UV-Vis is more suitable for monitoring the progress of the reducing reaction. MB dye reduction with 100 µL of NaBH4 (30 mm) alone without catalysts is limited to only 13%. The intensity at 664 & 676 nm of the MB and IE with 10 mg catalysts without $NaBH_4$, on the other hand, decreases up to 20% in about 6 min after abolition time, which is due to the adsorption of dye onto the catalyst.

3.1.10. *Photocatalytic and Adsorption Studies*

MB and IE removal depends on adsorption quantity, pH, and time. These three parameters were exploited by employing Fe_3O_4 towards MB and IE dye.

Adsorption of MB and IE on Fe_3O_4 was performed at rt in the dark and at natural pH 7. In another reaction vessel, 10 mg of adsorbent (Fe_3O_4) was taken in 100 mL of 20 ppm MB, and the next IE solution (20:80), 20 ppm, was prepared, which was again stirred along with Fe^{2+} at the same rpm by a magnetic stirrer. The amount of catalyst was filtered to remove the particles after a defined time period (1 mL aliquot) was withdrawn through a syringe. The amount of MB and IE predicted by using UV-Vis characteristic absorption peak for MB at 664 nm, and 668 nm for IE, was mixed in dye solution with the desired pH adjusted respectively with 0.1 M HCl or NaOH.

The amount of MB and IE adsorbed on MNPs is calculated in the following equation [55].

$$q = (Co - Ce)\frac{V}{m} \quad (1)$$

q quantity of dye adsorbed/unit of Fe_3O_4 (mg/g)
C_o – dye initial concentration (mg/L)
C_e – equilibrium dye concentration (mg/L)
V – solution volume (L)
m– Fe_3O_4 weight (mg)

$$\%\ adsorption = (C0 - Ci) \times \frac{100}{C0} \quad (2)$$

C_o & C_i -beginning and final dye concentration [56]. Photocatalytic experiment (in sunlight) in brief, 100 mL of both MB dye (20 ppm) and IE (20 ppm) in the presence of 10 mg Fe_3O_4 was electronically agitated under sunlight for 3 h after the system equilibrated by dark stirring for about 45 min before exposure to sunlight. The first one is given for the photodegradation rate of each individual experiment [57].

$$\%\ of\ photodegradation = (C0 - Ci) \times \frac{100}{C0} \quad (3)$$

Weak interaction of MB and IE in dark conditions, while a strong interaction with sunlight on Fe_3O_4 is noticed. Therefore, the adsorption of MB and IE dye is employed in sunlight. In UV-Vis, MB absorption was displayed at 297nm and 664nm, and IE appeared at 299nm to 676 nm, respectively. The absorbance intensity maximum in the UV region shows the presence of a high rate of π-π* transition (aromatic ring), and the absorbance maximum in the visible region displays the existence of n-π* transition based on the -N=N- group present in MB as well as IE. The adsorption/degradation efficiency of MB with iron oxide alone 90.34% and IE with iron oxide alone 88.93% observed. These studies elucidated that the prepared iron oxide showed properties of dye adsorption and was an effective photocatalyst for decolourization of the hazardous organic dyes through surface adsorption (Figure S9)

4. Adsorption kinetics

4.1.1. *Contact time*

The effect of contact time for the elimination of MB & IE dyes is available in Figure S10. A percentage MB and IE adsorption on Fe_3O_4 in dark/light condition carried out at 100 mL (20 ppm) dye solution [58]. The dark adsorption relatively slow rate was observed, in which only 40.56% of MB and IE was removed, while at light reaction conditions, the percentage decolourization achieved was 90.34 and 88.93%, respectively. Rapid change in the rates of adsorption takes place initially, due to all the sites on the adsorbent are empty, hence concentration of the solute high. This may result in a lower rate of adsorption, due to the reduced vacant sites on the adsorbent & dye concentration. This reduced adsorption suggests probable formation of a monolayer of MB and IE on the adsorbent.

4.1.2. *Variation of pH*

UV-Vis data displayed an anomaly sharp, enhanced loading proportion at pH most of the Fe_3O_4 surface shows more negative charges at pH 7, and more cationic MB dye to interact (Figure S13). The adsorption of MB does not change while above pH 7. MB being cationic could not compete with H^+ ions, and less amount adsorbed MB at pH=1-3, which explained that high protonation lead to reduction in the adsorption [59]. The pH is one of the essential factors affecting the adsorption of adsorbates onto the surface of materials based on the electrostatic interaction. When the pH of a solution is smaller than its pH_{PZC} value ($pH<pH_{PZC}$), the adsorption sites will be positively charged, which is thus available for the uptake of anions. By contrast, the adsorption sites will be negatively charged if pH is higher than its p_{HPZC} value and consequently the adsorption of cations is favourable. Then the absorbance intensity of MB after the adsorption *v/s* the wavelength decreases dramatically with the pH values from 2 to 3. It slightly falls when pH increases from 4 to 9 and reaches a maximum at pH 10 (see the black line in Figure S11). These results show that the changes in the pH values significantly affect the adsorption rate of the MB, because of the transition of the surface charge from the positive to negative regions that facilitates the adsorption of the cation.

4.1.3. *Pseudo 1st order kinetics*

Estimation of the adsorption dynamic model in first-order pseudo kinetic adsorption for MB & IE on the catalyst surface was performed (Figures 12, 13). These are governed by the model given in equations 4 and 5, respectively [60]. The first-order pseudo plot showed a better linearity (R_2 near to unity), than the second-order pseudo- model, which was evidenced by R_2 and shown in Table 2, and commonly these reactions have a pseudo-first order kinetic, because one of the reactants is in the solid phase.

$$\log(q_e - q_t) = \log q_e - \frac{k_1}{2.303} t \quad (4)$$

$$\frac{t}{q_t} = \frac{1}{h} + \frac{1}{q_e} \quad (5)$$

qt (mg g^{-1}) and q_e (mg g^{-1}) are the MB amount adsorbed at time t (min) and in equilibrium.

4.1.4. *Pseudo 2nd order kinetics*

K_1 (min^{-1}) first-order pseudo rate constant, h [mg/ (g min)] initial adsorption rate in second-order pseudo-equation [61], and evaluated as $h=K_2 qe^2$. K_2g (mg. min) (Figures S20 & S14).

4.1.5. *Intraparticle diffusion*

In the light reaction condition, intraparticle diffusion of MB on Fe_3O_4 NPs was analysed, and revealed that the diffusion rate mainly depends on the quantity of catalyst used [62].

It was observed that the rate constant remains the same with the amount of catalysts increased (Figure S15). The model pseudo second-order (qe, cal) is the most suitable to adsorption process, and complexation reaction may be the rate controlling step (Table 2**).**

Table 2. Kinetic values of MB and IE.

Catalyst	I order	II order	Intra particle size
Fe_3O_4 (MB)	q_e (m_g g^{-1}) = 58.82 k_1 (min^{-1}) × 10^{-3}=0.027 R^2 = 0.9996	q_e (m_g g^{-1}) =0.4 K_2 (min^{-1}) × 10^{-3}=10.2 R^2 =-0.480	C (mg/g) =2.9 k_{id} (g mg^{-1} min^{-1}/2) =1.1 R^2 =0.9
Fe_3O_4 (IE)	q_e (m_g g^{-1}) =54.8 k_1 (min^{-1}) × 10^{-3}=0.021 R^2 = 0.991	q_e (m_g g^{-1}) =0.9 K_2 (min^{-1}) × 10^{-3}=14.5 R^2 = -0.257	C (mg/g) =7.3 k_{id} (g mg^{-1} min^{-1}/2) =0.2 R^2 =0.81

4.2. Isotherm Adsorption

4.2.1. *Langmuir*

Herein, we monitored the Langmuir isotherm for the adsorption capacity of Fe_3O_4 NPs on MB and IE in light reaction conditions (Figures S16 & S17). This is a theoretical construct, valid only for the monolayer formation of the surface on the adsorbent. Therefore, the Langmuir model is an adsorption model, in other words, the binding or distribution of metal ions between the liquid and solid phases, represented as [63-67].

$$q_e = q_m K_L \cdot \frac{Ce}{1} + K_L C_e \quad (6)$$

q_m and K_L are Langmuir constants
Langmuir linear isotherm

$$\frac{1}{q_e} = \frac{1}{q_m} + \frac{1}{q_m} K_L C_e \quad (7)$$

C_e= concentration equilibrium (mg/L)
q_e= MB adsorbed (mg/g)
q_m= extreme quantity of adsorption (mg/g)
K_L= equilibrium sorption constant (L/mg)
q_m and K_L values calculated by slope-intercepted Langmuir plot of $1/q_{ev}$/s $1/C_e$ (Table 3)
The translation of the adsorption rate follows the Langmuir-Hinshelwood equation, which is expressed below.

$r = K_a K_c C_0 / 1 + K_a C_0$

Where K_a = adsorption constant,
K_c = specific rate constant, and
C_0 = initial concentration.
and then photo excited species are reacted with dye which supersedes it into an intermediate species on the surface of the defect. The intermediate compound then either further harms products or recombines with electrons.The following is the reaction scheme for the removal of dye.

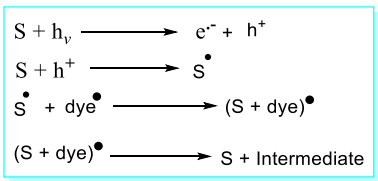

In this reaction *hv* is the amount of light, 'S' is the surface the catalyst e. - and h. are the electron and hole, respectively (Figure 11).

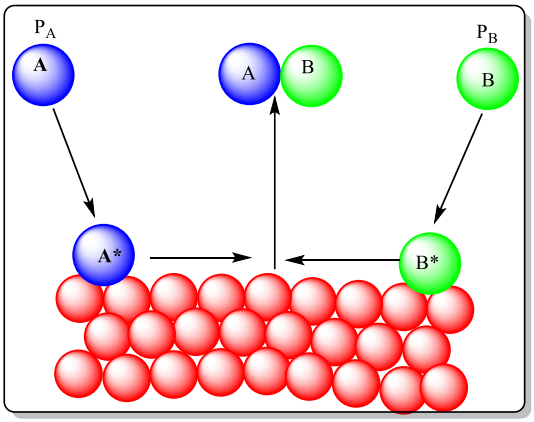

Figure 11. Illustration of adsorption phenomena by the Langmuir mechanism

4.2.2. *Freundlich*

Isotherm Freundlich conducted under light & dark conditions at rt as illustrated in Figures S18 & S19. In the development of adsorption theories, Freundlich isotherm was the first to be formulated and it applies heterogeneous adsorbent surface both single as well as multilayer sorption. Freundlich isotherm offers the representation equation [67-70].

$$q_e = K_F Ce^{1/n} \quad (8)$$

K_F= constant Freundlich isotherm (mg/g), n= intensity of adsorption, C_e= concentration of adsorbate at equilibrium (mg/L), q_e= adsorbed amount/g at equilibrium (mg/g).
Freundlich linear isotherm

$$\ln q_e = \ln K + \frac{1}{n} \ln C_e \quad (9)$$

n & K_F values calculated plot of l_{nqe} v/s ln C_e (Table 3).

4.2.3. *Adsorbent product characterization by HR-MS*

The adsorbed dye on the catalysts was washed with water and alcohol after sunlight exposure, then concentrated to decrease in volume, and the final residue was evaluated by HR-MS. MB & IE were analysed

separately, and spectra shown in Figures 12,13. These data revealed the main peak at 320.11 Da and 319.85Da is refer to of MB and IE molecular weight, respectively after exposure to sunlight for 3h. Thus, the negative charge on active surface of the catalysts electrostatically interacts with the dye of positively charged MB adsorbed faster than degradation of the dye.

Adsorption v/s Degradation

Adsorption is the process where molecules attached to the surface of the catalysts. Degradation, on the other hand involves breakdown of a molecule into smaller fragments. HR-MS used to analyze both, and revealed intact mass of the dye.

Table 3 . model fitting results for MB isotherm adsorption on the catalyst

Catalyst	Freundlich	II order
Fe_3O_4 (MB)	K_F=7.51 1/n = 0.68 R^2 = 0.863	q_m (mg/g) =218.5 K_L (L/m_g)=0.011 R^2 =0.983
Fe_3O_4 (IE)	K_F =6.33 1/n = 0.50 R^2 =0.854	q_m (mg/g) =210.2 K_L (L/m_g) =1.890 R^2 = 0.98

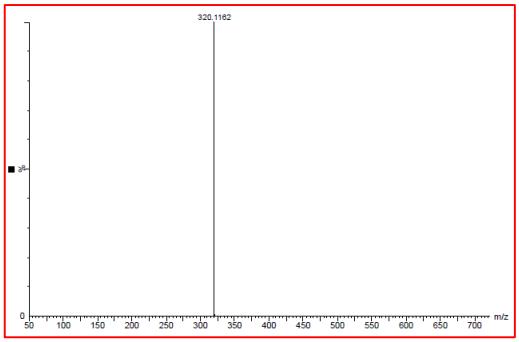

Figure 12. HR -MS Spectra of MB adsorbent

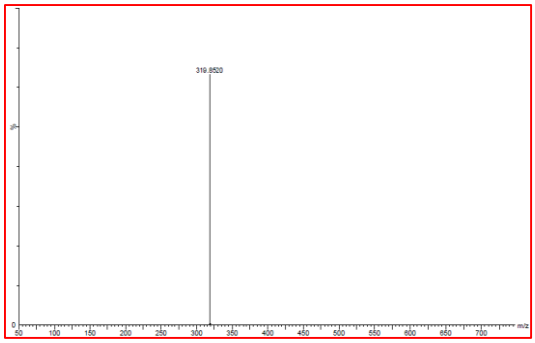

Figure 13. HR -MS Spectra of IE adsorbent

4.2.4. *Adsorption mechanism*

The adsorption process is facilitated by various factors, including high surface area, high surface charge, and the presence of functional groups. Accordingly, the FT-IR spectrum of Fe_3O_4, as shown in Figure 1, bands at 1629 cm^{-1} and 3435 cm^{-1} are related to the presence of hydroxyl groups and attributed to OH-bending and OH-stretching, respectively. The peaks between 1157.29 cm^{-1} and 1114.86 cm^{-1} are assigned to the stretching of between C-O and O-H for -COOH. Therefore, the phenolic and carboxylic groups played key roles in the adsorption mechanism. In addition, the mechanisms of MB removal by the Fe_3O_4 adsorbent are illustrated in Scheme 4. The bonding of hydrogen between the -OH groups of the Fe_3O_4 and the aromatic heterocyclic ring of the MB was a significant contributor in capturing the MB. The *Vander Waals* forces between the phenolic ring of the adsorbent and aromatic heterocyclic ring of the MB may also have contributed. The batch study data pointed out that Fe_3O_4 exhibited better dye removal efficacy with a higher solution pH.

This is possibly due to electrostatic interactions, because at a higher pH, the surface of the Fe_3O_4 tends to be negatively charged and interacts favourably with the positively charged MB dye. Thus, MB molecules were captured from water through *Vander Waals* forces, hydrogen bonding, and the electrostatic interaction.

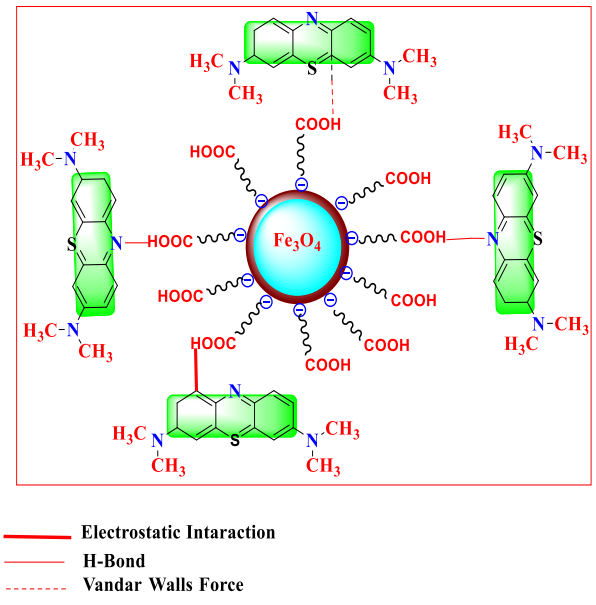

Scheme 4. Proposed adsorption mechanisms of MB on Fe_3O_4

5. Conclusion

The present work describes the synthesis of Fe_3O_4 nanoparticles employing a biogenic approach, and characterized using UV-Vis, FT-IR, XRD, HR-TEM, FE-SEM, and VSM. The prepared iron oxide is used further to remove toxic organic dyes (MB & IE) from industrial and laboratory settings. The catalysts employed involved the decolourization of the dye MB and IE, as confirmed by HR-MS, and the amount of dye removal of MB (90.34%) and IE (88.93 %) in the presence of iron oxide under sunlight. The data suggested that the prepared MNPs biogenic excelled in very good adsorption of the dye based on primary and secondary electronic interactions.

Acknowledgement

Author Dr. KK is thankful to the SERB-SURE, GOI (SUR/2022/002631) and RCUB (RCU-IDR-2022-23) for financial support.

Ethics declarations

Ethics and Consent to Participate

Not applicable.

Competing Interests

The authors declare no competing interests.

Funding

Not applicable.

Supplementary information

FT-IR, ^{1}H-, ^{13}C-NMR and LC-MS of the selected compounds are available in supplementary.

Authors Contribution
All authors have contributed equally to prepare the paper.

Availability of data and materials
The data supporting the findings of the article are available within the article.

Conflict of interests
The authors have declared no conflict of interest.

References

[1] M. A. Pandit, S. Billakanti, K. Muralidharan, J. Envier. Chem. Eng., 19 (2019) 30665-7.
DOI: https://doi.org/10.1016/j.jece.2019.103542

[2] X. Xiong, H. Zhang, R. Wang, Z. Tang, M. Yang, ACS EST Water., 3 (2015) 4752-4952.
DOI: https://doi.org/10.1021/acsestwater.4c00169

[3] S. Dutta, B. Gupta, S. K. Srivastava, A. K. Gupta Mater. Adv., 2 (2021) 4497-4531.
DOI: https://doi.org/10.1039/D1MA00354B

[4] I. M. Banat, P. Nigam, D. Singh, R. Marchant, Bioresour. Technol., 58 (1996) 217-227.
DOI: https://doi.org/10.1016/S0960-8524(96)00113-7

[5] A. F. Perez, G. Marban, *ACS Omega 5 (*2020**)** 29801-29815.
DOI: https://doi.org/10.1021/acsomega.0c03830

[6] L. Y. Zhanga, W. Zhanga, Z. Zhoua, C. M. Li, J. Colloid Interface Sci. 476(2016)200–205.
DOI: http://doi.org/10.1016/j.jcis.2016.05.025

[7] H. Langhals, Angew. Chem. Int. Ed., 43 (2004) 5291-5292.
DOI: https://doi.org/10.1002/anie.200485174

[8] S. Karishma, P. R. Yaashikaa, P. Senthil Kumar, R. Kamalesh, A. Saravanan, G. Rangasamy Environ. Sci.: Adv., 2 (2023) 1488-1504.
DOI: https://doi.org/10.1039/D3VA00194F

[9] A. N. Ejhieh, S. Khorsandi, j of ind. Eng. Chem., 5 (2013) 10-35.
DOI: http://dx.doi.org/10.1016/j.jiec.2013.06.026

[10] I. K. Konstantinou, T. A. Albanis, Appl. Catal., B, 49 (2004) 1-14.
DOI: https://doi.org/10.1016/j.apcatb.2003.11.010

[11] N. Singh, B. R. Goldsmith, ACS Catal.10 (2020) 3365−3371.
DOI: https://doi.org/10.1021/acscatal.9b04167

[12] A. Bafana, S. S. Devi,T. Chakrabarti, Environ. Rev, 19 (2011) 350-371.
DOI: https://doi.org/10.1139/a11-018

[13] V. P. Dinh, T. Diem, RSC Adv., 9 (2019) 25847-25863.
DOI: https://doi.org/10.1039/c9ra04296b

[14] M. Afzal, K. Rehman, G. Shabir, R. Tahseen, A. Ijaz, A. J. Hashmat, H. Brix, npj Clean Water 2 (2019) 3.
DOI: https://doi.org/10.1038/s41545-018-0025-7

[15] K. L. Offenbaume, E. Bertone, R. A. Stewart, *Water 12* (2020) 2591.
DOI: https://doi.org/10.3390/w12092591

[16] T. Yahagi, M. Degawa, Y. Seino, T. Matsushima, M. Nagao, T. Sugimura,Y. Hashimoto, Cancer Lett, 1 (1975) 91-96.
DOI: https://doi.org/10.1016/S0304-3835 (75)9563-9

[17] S. Nam, V. Renganathan, Chemosphere, 40 (2000) 351-357.
DOI: https://doi.org/10.1016/S0045-6535(99)00226-X

[18] P . Singh, A. Sarswat, U. Charles J. Pittman, M. Todd, D. Mohan, ACS Omega., 6 (2020) 2575-2593.
DOI: https://doi.org/10.1021/acsomega.9b02842

[19] B. J. Singh, A. Chakraborty, R. Sehgal J. Environ. Manag. 348 (2023) 119230.
DOI: https://doi.org/10.1016/j.jenvman.2023.119230

[20] R. A. Tohamya, S. S. Alia, F. Li, K. M. Okasha, Y. A. G. Mahmoud, T. Elsamahya, H. Jiaoa, Y. Fua, J. Sun, Ecotoxicol. Environ. Safety 231 (2022) 113160.
DOI: https://doi.org/10.1016/j.ecoenv.2021.113160

[21] M. J. Prival, S. J. Bell, V. D. Mitchell, M. D. Peiperl, V. L. Vaughan, Mutat. Res., 136 (1984) 33- 47.
DOI: https://doi.org/10.1016/0165-1218(84)90132-0

[22] L. He, F. Michailidou, H. L. Gahlon, W. Zeng Chem. Res. Toxicol. 35 (2022) 901−915.
DOI: https://doi.org/10.1021/acs.chemrestox.1c00427.

[23] R. A. Tohamy, S. S. Ali, F. Li, K. M. Okasha, Y. A. G. Mahmoud, T. Elsamahy, H. Jiao, Y. Fu, J. Sun, Ecotoxicol. Environ. Safety 231 (2022), 113160.

DOI: https://doi.org/10.1016/j.ecoenv.2021.113160

[24] S. Sansuk, S. Srijaranai, Environ. Sci. Technol., 50 (2016) 6477-6484.
DOI: https://doi.org/10.1021/acs.est.6b00919

[25] S. Parlayıcı, E. Pehlivan, Int. J .Phytoremediation, 23 (2021) 26.
DOI: https://doi.org/10.1080/15226514.2020.1788502

[26] M. Rezaei, A. N. Ejhieha, inter j. hydro. Ener., 45 (2020) 24749e-2476430.
DOI: https://doi.org/10.57647/j.ijc.20251503.26

[27] L. Wu, X. Liu, G. Lv, R. Zhu, L. Tian, M. Liu, Y. Li, W. Rao, T. Liu & L. Liao, Sci Rep, 11 (2021) 10640.
DOI:10.1038/s41598-021-90235-1

[28] E. A. Alabbad, Open Chem J, 7 (2020) 16.
DOI: https://doi.org/10.2174/1874842202007010016

[29] B. Tunçsiper, J Clean Prod, 228 (2019) 1368.
DOI: https://doi.org/10.1016/j.jclepro.2019.04.211

[30] K. S. Bharathi, S. T. Ramesh, Appl Water Sci, 3 (2013) 773.
DOI: https://doi.org/10.1007/s13201-013-0117-y

[31] Y. Dai, Q. Sun, W. Wang, L. Lu, M. Liu, J. Li, S. Yang, Y. Sun, K. Zhang, J. Xu, W. Zheng, Z. Hu, Y. Yang, Y. Gao, Y. Chen, X. Zhang, F. Gao, Y. Zhang, Chemosphere, 211 (2018) 235.
DOI: https://doi.org/10.1056/NEJMoa1300955

[32] M. R. Panuccio Sorgonà, A. M. Rizzo, G. Cacco, J Environ Manage, 90 (2009) 364.
DOI: https://doi.org/10.1016/j.jenvman.2007.10.005

[33] Huang X, Gao N Y & Zhang Q L, Thermodynamics and kinetics of cadmium adsorption onto oxidized granular activated carbon, J Environ Sci, 19 (2007) 1287.
DOI: https://doi.org/10.1016/s1001-0742(07)60210-1

[34] T. J. Bamgbose, S. Adewuyi, O. Bamgbose & A. A. Adetoye, Afr J Biotechnol, 9 (2010) 2560.
DOI: https://doi.org/10.1016/1021-9986/15/3/25

[35] Hizal J & Apak R, Modeling of cadmium (II) adsorption on kaolinite-based clays in the absence and presence of humic acid, Appl Clay Sci, 32 (2006) 232.
DOI: https://doi.org/10.1016/j.clay.2006.02.002

[36] Panda G C, Das S K & Guha A K, Biosorption of cadmium and nickel by functionalized husk of Lathyrussativus, Colloids Surf B, 62 (2008) 173.
DOI: https://doi.org/10.1016/j.colsurfb.2007.09.034

[37] S. J. Peighambardoust and R. Foroutan, S. H. Peighambardoust, H. Khatooni and B. Ramavandi, Chemosphere, 282 (2021) 131088.
DOI: https://doi.org/10.3390/ma15196964

[38] V. K. Gupta and A. Nayak, Chem Eng J, 180 (2012) 81.
DOI: https://doi.org/10.1016/j.cej.2011.11.006

[39] R. Jiang, J. Tian, H. Zheng, J. Qi, S. Sun and X. Li, J Environ Manage, 155 (2015) 24.
DOI: https://doi.org/10.1039/d3ra00723e

[40] D. M. Patil, K. T. Chandrashekara, J. Manjannaa, M. Sridhara. Iranian Journal of Catalysis 13 (1) 2023 47-5.
DOI:https://doi.org/10.30495/IJC.2023.1972239.1972

[41] P. Anitha, A. Ramachandran, R. Sudha, N. Valarmathi and D. Geetha, Indian J Chemical Techn, 31 (2024) 355-368.

[42] K. Saeed, I. Khan, T. Gul, M. Sadiq, Appl Water Sci. 7 (2017) 3841–8.
DOI: https://doi.org/10.1007/s10854-020-03431-6

[43] M. Valaskova, J. Tokarsky, J. Pavlovsky, T. Prostejovsky, K. Kocí. Materials. (2019) 121880.
DOI: https://doi.org/10.1007/s40201-020-00563-z

[44] Y. Liu, N. Sun, J. Hu, S. Li, G. Qin, R Soc Open Sci. 5 (2018) 172196.
DOI: https://doi.org/10.1016/j.addma.2022.102691

[45] T. Ma, L. Zheng, Y. Zhao, Y. Xu, J. Zhang, X. Liu, ACS Appl Nano Mater. 2 (2019) 2347–57.
DOI: https://doi.org/10.1021/acsami.0c13070

[46] D. M. S. N. Dissanayake, M. M. M. G. P. G. Mantilaka, T. C. Palihawadana, G.T.D. Chandrakumara, R.T. D. Silva, H. M. T. G. A Pitawala, K.M.N Silva, G. A. J Amaratunga. RSC Adv. 9 (2019) 21249–212257.
DOI: https://doi.org/10.1039/C9RA03756J

[47] Y. Ge, M. Hoque, Q. Qu. Electrochem Energy Technol. 5(2019) 1–6.
DOI: https://doi.org/10.1201/9781003145585-5

[48] J. Kim, J. Hwang, Y. Sun. J. Hassoun9, Sustain Energy Fuels. 3(2019) 2675–87.
DOI. https://doi.org/10.1039/C8SE00442K

[49] V. Harnchana, S. Chaiyachad, S. Pimanpang, C. Saiyasombat, P. Srepusharawoot, V. Amornkitbamrung, Sci Rep. 9 (2019).
DOI: https://doi.org/10.1007/s40201-020-00563-z

[50] G. Darmograi, B. Prelot, A. Geneste, G. Martin-Gassin, F. Salles, J. Zajac, J. Phys. Chem. C. 120 (2016) 10410-10418.
DOI: https://doi.org/10.1021/acs.jpcc.6b01888

[51] Z. Li, B. Yang, S. Zhang, B. Wang, B. Xue, J. Colloid Interface Sci. 12 (2014) 10202- 10210.
DOI: https://doi.org/10.1039/C4TA01028K

[52] M. Del Arco, S. Gutierrez, C. Martin, C. V. Rives, Phys. Chem. 3 (2001) 119-126.
DOI: https://doi.org/10.3390/chemengineering6040060

[53] N. B. H. Abdelkader, A. Bentouami, Z. Derriche, N. Bettahar, L. C. De Menorval, J. Chem. Eng., 169 (2011) 231-238.
DOI: https://doi.org/10.1039%2Fd0ra04898d

[54] J. Bai, Y. Liu, X. Yin, H. Duan, J. Ma, Appl. Surf. Sci. 416 (2017) 45-50.
DOI: https://doi.org/10.1039/C7RA07417D

[55] F. T. Zhang, X. Long, D. W. Zhang, Y. L. Sun, Y. L. Zhou, Y. R. Ma, L. M. Qi, X. X. Zhang, Sens. Actuators B Chem., 192 (2014) 150-156.
DOI: https://doi.org/10.1016/j.snb.2013.10.097

[56] M. Luaibi, M. A. Atiya, A. K. Hassan, Z. A. Mahmoud, *Karbala Int. J. Mod. Sci*.8 (2022) 9e28.
DOI: http://dx.doi.org/10.33640/2405-609X.3217

[57] Y. Gao, W. Zhu, J. Li, W. Liu, X. Li, J. Zhang, T. Huang, J. Environ. 121 (2022) 148-158.
DOI: https://doi.org/10.1016/j.jes.2021.09.024

[58] N. Semwal, D. Mahar, M. Chatti, A. Dandapat, M. C. Arya, Heliyon 9 (2023) e22027.
DOI: https://doi.org/10.1016/j.heliyon.2023.e22027

[59] D. G. Strawn, *Soil Syst.* 5 (2021) 13.
DOI: https://doi.org/10.3390/soilsystems5010013

[60] O. P. Murphy, M. Vashishtha, P. Palanisamy, K. V. Kumar ACS Omega 8 (2023) 17407−17430.
DOI: https://doi.org/10.1021/acsomega.2c08155

[61] Y. Wang, Z. Wang, Y. Rui, M. Li, Biosens. Bioelectron., 64 (2015) 57-62.
DOI: https://doi.org/10.1016/j.bios.2014.08.054

[62] A. Safavi, S. Momeni, Biosens. Bioelectron., 201 (2012) 125–131.
DOI: http://dx.doi.org/10.1016/j.molliq.2016.08.058

[63] M. Zhu, G. Diao, J. Phys. Chem. C. 115 (2011) 18923–18934.
DOI: https://doi.org/10.1021/jp052678c

[64] H. Veisi, S. Razeghi, P. Mohammadi, S. Hemmati, Mater. Sci. Eng. C. 97 (2019) 624-631.
DOI: https://doi.org/10.1039/C9RA08809A

[65] S. Rahim Pouran, A. Bayrami, A. R. A. Aziz, W. M. A. W. Daud, M. S. Shafeeyan, J. Mol. Liq., 222 (2016) 1076–1084.
DOI: https://doi.org/10.48175/594

[66] N. Jaafarzadeh, A. Takdastan, S. Jorfi, F. Ghanbari, M. Ahmadi, G. Barzegar, J.Mol. Liq., 256 (2018) 462–470.
DOI: https://doi.org/10.1016/j.molliq.2018.02.047

[67] J. Saffari, N. Mir, D. Ghanbari, K. Khandan-Barani, A. Hassanabadi, M. R. Hosseini-Tabatabaei, J. Mater. Sci. Mater. Electron. 26 (2015) 9591-9599.
DOI: https://doi.org/10.1088/1755-1315/276/1/012059

[68] G. C. Silva, V. S. T. Ciminelli, A. M. Ferreira, N. C. Pissolati, P. R. P. Paiva, J. L. Lopez, Mater. Res. Bull., 49 (2014) 544–551.
DOI: https://doi.org/10.1039/D3NA00754E

[69] K. Pakzad, H. Alinezhad, M. Nasrollahzadeh, Ceram. Int. 45 (2019) 17173–17182.
DOI: https://doi.org/10.1016/j.btre.2020.e00518

[70] R. Shekhanavar, S. Y. Khatavi, A. Kamanth, K. Kantharaju, Iranian Journal of Catalysis OC-2306-2812.